X-RAY SOURCE BASED ON THE PARAMETRIC X-RAYS MECHANISM

A. Lobko, O. Lugovskaya

Institute for Nuclear Problems, Belarus State University

Prospects of parametric x-rays (PXR) application for the development of a tuneable quasi-monochromatic x-ray source for medical imaging are discussed. Analysis of basic requirements for electron accelerator shows that it must be relatively low-energy and high-current linac. In comparison with known ultra-relativistic cases, at low energies PXR properties will be modified to a great extent by multiple scattering of electrons. PXR intensity dependences on target thickness and beam energy are calculated taking multiple scattering into account. It is concluded that PXR source based on real medical accelerators is feasible and can provide x-ray flux needful for obtaining high quality medical images.

1. INTRODUCTION

Parametric x-rays (PXR) produced by a relativistic charged particle uniformly moving through a single crystal were claimed as a very attractive radiation mechanism for x-ray source since its theoretical prediction in 1972 [1—3] and first experimental observation in 1985 [4]. Actually, it has a number of indisputable features, namely, high monochromaticity, energy tuneability, polarization, directivity, and possibility to be emitted to large angles relative to beam direction, i.e. provide monochromatic x-rays virtually free of background. PXR properties were studied at a number of accelerator facilities worldwide but a PXR-based x-ray source is still not developed.

Evidently, this is connected with the fact that PXR research is performed at existing linear and annular accelerators and limited by their technical specifications. So, we should recognize how to design a PXR-based source that will meet the consumer's requirements for its use in industry and medicine.

Industry and science, as consumers, essentially yield to medicine, which represents the huge market for devices and methods for x-ray diagnostics. Statistically, x-ray devices count for about 60 % of medical diagnostics devices [5]. Despite the development of alternative diagnostics methods, e.g. ultrasound and magnetic resonance imaging, the number of studies in the field of x-ray diagnostics remains high. First of all, medicine demands decreased irradiation doses, together with increased resolution and contrast. These requirements can be met if the customer will be offered a monochromatic tuneable source, providing x-radiation with exactly the energy required for examination of a specific organ. For example, in mammography the maximum spectral density lies in the range of 17—20 keV; in radiography of the chest, extremities and head, the range of 40—50 keV is optimal; while the 50—70 keV range is used for abdomen and pelvis radiography. Precise selection of monochromatic radiation energy will allow a reduction of a patient dose of tens times, even in comparison with digital radiography and computer tomography, with improvement of x-ray image quality. However, in comparison with scientific and industrial applications where signal accumulation is possible, in the case of medicine the source should emit number of quanta sufficient to provide necessary contrast of an image at the specific value of the signal-to-noise ratio. Estimations [6, 7] give minimal value of x-ray quanta necessary for high-quality image equal to ~10^7 photons/mm^2. PXR quantum yield in a thin crystalline target even at high enough (900 MeV) beam energy is not very large and amounts only ~10^{-5}—10^{-6} photons/e$^-$·sr [8]. Assuming the target to be imaged is 30 cm diameter at one meter distance from a

source, it is necessary to apply ~0.1 A current to get a required x-ray flux. Such currents can be achieved only in low energy accelerators. Though theoretically PXR may be emitted at any energy of charged particles [9], there is a factor limiting the minimal value of beam energy for source under discussion. Assuming x-ray energy necessary for subtractive coronary angiography $\varpi_B = 33$ keV then the angle of radiation θ_B in a diamond target will come to ~4° for (111) reflex and ~7° for (220) reflex. That it is enough for arrangement of a patient at 1—2 meter distance from the target. Now let us estimate energy E_p of an electron beam providing angular width of reflex [10] $\vartheta_{ph}^2 = |\chi_0'| + \gamma^{-2} + \overline{\theta_s^2}$ ($|\chi_0'|$ — Fourier component of a crystal dielectric constant, $\gamma = E_p / mc^2$, $\overline{\theta_s^2}$ — mean-square angle of multiple scattering) equal ~5°, i.e. energy at which x-ray reflex and forward background are still separated from each other and the radiation in which we are interested keeps all the properties necessary for a medical source. The dominant component here is the mean-square angle of multiple scattering $\overline{\theta_s^2}$ and lowest estimation of beam energy gives a value ~17 MeV. To provide more real evaluations for PXR source based on low-energy electron beam, we should look into multiple scattering (MS) of electrons more precisely, because MS appeared to be the most significant factor affecting PXR intensity and angular distribution at relatively low energies and/or thick targets [8]. In low energy cases we shouldn't use kinematics formulae [10], where MS is considered phenomenologically. Let us describe the multiple scattering influence on x-ray reflex characteristics following [11] in more detail.

2. CALCULATION OF X-RADIATION PROPERTIES IN THE MULTIPLE SCATTERING PRESENCE

To get an expression for spectral-angular density of radiation with MS account, it is necessary to average the squared modulus of all possible particle trajectories in a crystal in the following expression [12, 13]

$$\frac{d^2N_s}{d\varpi d\Omega} = \frac{e^2Q^2\varpi}{4\pi^2\hbar c^3}\left|\int_{-\infty}^{+\infty} \vec{v}\vec{E}_{\vec{k}}^{(-)s}(\vec{r}(t), \varpi \exp(-i\varpi t)dt\right|^2 \quad (1).$$

The obtained expression will describe all mechanisms of the radiation: PXR, *Bremsstrahlung*, and transition radiation in a single manner. The velocity vector is presented in the form: $\vec{v} = \vec{v}_0 \cos\theta + v_0\vec{\theta}$ (where $\vec{v}_0$ determines the direction of the initial velocity of a charged particle, $\theta \equiv |\vec{\theta}|$ — the angle of multiple scattering of a particle ($\theta << 1$), $\vec{\theta}$ — two-dimensional vector, $\vec{\theta} \perp \vec{v}_0$ and $\vec{\theta} = 0$ at $t \le 0$).

Averaging is followed [13], where the procedure was performed with the help of dispersion function, satisfying the Fokker—Planck kinetic equation in the amorphous medium. Averaging of the right part of the equation (1) was performed and the integral expressions for spectral-angular distributions of the radiation, taking into account multiple scattering for the lateral and forward PXR maximums were derived.

Selected functions of the particle distributions on coordinates and angles are usually applied in calculations of *Bremsstrahlung* intensity of ultra-relativistic electrons in amorphous media. It is applicable if direction of vector of a charged particle initial velocity does not coincide with directions of the basic crystallographic axes or planes. Also, one can ignore the influence of crystal structure on charged particles trajectories and apply dispersion functions of amorphous medium when value of initial angular divergence of a particle beam, falling on the crystal along the direction of main crystallographic axes or planes, satisfies the inequality $|\Delta\vec{v}_0| / c > \sqrt{(2U_0 / E_p)}$, where U_0 — potential of atomic axis or plane, E_p — particle energy. In this case during the passage of charged particles through the crystal, orientational effects will be expressed less strongly than in the case of a well-collimated beam, and the averaging of (1) over simple dispersion functions ensures a satisfactory approach.

It is necessary to note, that in the case, when the value $|\Delta\vec{v}_0 / c| < \left(\gamma^{-2} + \frac{\omega_L^2}{\omega_B^2}\right)^{-1/2}$ ($\omega_B^{(n)} = \frac{\pi cn}{d\sin\theta_B}$, n=1, 2, 3... — Bragg frequency, θ_B — angle between the particle velocity vector $\vec{v}_0$ and planes corresponding to the vector $\vec{\tau}$, ω_L — Langmuir frequency of a crystal), it is not required to make additional averaging in (1) on the initial divergence of the vector direction $\vec{v}_0$.

There are two factors limiting the longitudinal size of quasi-Cherenkov radiation formation area: MS of charged particles on atoms of substance and x-ray absorption in the medium. As in case of radiation generation in an amorphous medium, the PXR characteristics essentially depend on the relation between crystal thickness along the direction of the charged particle movement L_0 and *Bremsstrahlung* coherent length L_{Br}. The theory of PXR with the phenomenological account of MS influence on particle energy range exceeding threshold energy $E_{tr} = mc^2 \left|\chi_0'\right|^{-1/2}$ is in good agreement with experimental results only at crystal thickness $L_0 << L_{Br}$. In this case MS influence appear only as a small addition in the intensity of generated x-ray caused by *Bremsstrahlung*. Also MS influence on PXR phase is taken into account and interference between PXR and *Bremsstrahlung* is neglected. In the inverse case MS essentially changes the parameters of PXR itself.

3. PXR CHARACTERISTICS DEPENDENCE ON CRYSTAL TARGET THICKNESS

To demonstrate MS effect on PXR characteristics, numerical calculations were performed for following conditions: target Si (220) in Laue geometry, $2\theta_B = 19^\circ$, electron beam energy 900 MeV.

PXR spectral-angular density as a function of crystal target thickness is shown in Fig. 1. It is evident, that already at $L_0 \sim L_{Br}$ presence of MS results in PXR intensity distinctly less than intensity determined without MS account. During further increase of the crystal thickness, spectral-angular density achieves saturation at thickness of $\sim 2-3 \cdot L_{Br}$ and then goes down. It is seen from this figure that PXR spectral-angular density without MS (curve 1) continues to grow with crystal thickness increase even up to $\sim 10 L_{Br}$. The tendency shows that absorption still does not plays an essential role though L_0 becomes of the order of L_{abs}. Simultaneously with the variation of PXR spectral-angular density with crystal thickness increase, change of its spectral width appears (see Fig. 2). As long as the thickness of the crystal target does not exceed $0.5 L_{Br}$, spectral-angular density and spectral width of PXR reflex determined with MS account practically agree with the values received without MS consideration. At the same time, spectral width of PXR peak decreases with L_0 increase. The width of PXR maximum is inversely proportional to radiation coherent length. As the target thickness increase (on thickness of ~ L_{Br} and larger) PXR coherent length begins to be limited by L_{Br}. So, PXR peak width without MS continues to decrease with L_0 growth, but MS account results in stabilization of peak width at $L_0 \sim L_{Br}$ (Fig. 2).

Thus, calculation results, demonstrated in Figures 1 and 2, show that MS of a charged particle results not only in radiation phase shift, but also in essential decrease of PXR spectral-angular density at angles of $\vartheta \sim \vartheta_{ph}$ as well as in change of reflex width, even in case of $L_0 \sim L_{Br}$.

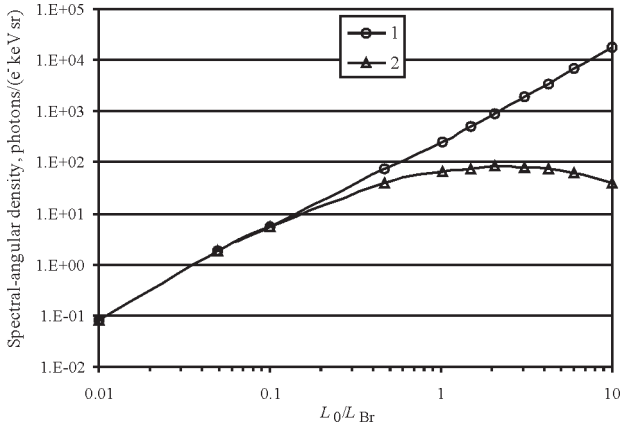

Fig. 1. Dependence of PXR spectral-angular density on crystal thickness, counted along a direction of charged particle movement in units of L_{Br}: 1 — without MS account, 2 — with MS account

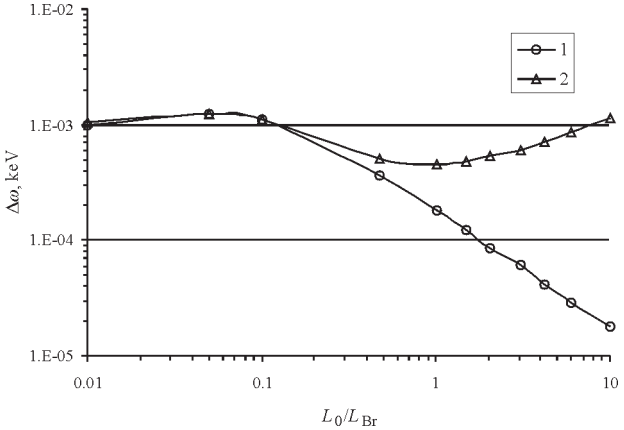

Fig. 2. Dependence of PXR frequency half-width on crystal thickness, counted along a direction of charged particle movement in units of L_{Br}: 1 — without MS account, 2 — with MS account

As a result of joint processes of PXR spectral narrowing and spectral-angular density decrease, PXR integral characteristics do not vary essentially. As an example, in Fig. 3 dependences of PXR angular distribution (at $\vartheta = 1.66 \cdot 10^{-3}$ rad) on crystal thickness without MS (1) and in the MS presence (2) are given. One can see that for target thickness of $L_0 = 10 L_{Br}$ value of spectral-angular distribution (at $\vartheta = 1.66 \cdot 10^{-3}$ rad) calculated without MS account exceeds the value received with MS account more than by two orders of magnitude (compare with Fig. 1), while amplitudes of angular distributions (for the same angle) differ less than by one order (Fig. 3). MS also results in PXR angular distribution spreading, therefore if the angular aperture of a detector is big enough ($\theta_D >> \vartheta_{ph}$), the difference in results for integrated number of the quanta calculated with the MS account and without taking it into account will be even less, than for angular distributions. Thus, the most significant difference of the results received with and without MS account is observed for differential distributions.

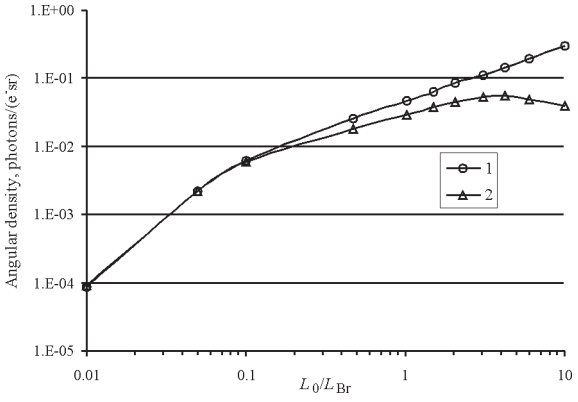

Fig. 3. Dependence of PXR angular density maximum on crystal thickness, counted along a direction of charged particle movement in units of L_{Br} (integration on frequency on half-width of PXR spectral-angular density distribution): 1 — without MS account, 2 — with MS account

4. PXR INTENSITY DEPENDENCE ON CHARGED PARTICLE ENERGY

As well as for Cherenkov radiation in a homogeneous media, PXR spectral-angular density has well-marked threshold behaviour. However, due to essential dispersion of a crystal refraction index, dependence of integral PXR intensity on particle energy is relatively smooth. It is differs in $E_p << E_{tr}$ and $E_p >> E_{tr}$ energy regions, where threshold energy $E_{tr} = mc^2 \gamma_{tr}$, $\gamma_{tr} = \sqrt{|\chi_0'|} \approx \frac{\omega_B}{\omega_L}$. So, PXR quantum yield at particle energy $E_p << E_{tr}$ is $N^{PXR} \sim \left(\frac{E_p}{E_{tr}}\right)^4$ and $N^{PXR} \sim \ln\left(\frac{E_p}{mc^2}\right)$ at $E_p >> E_{tr}$. Note, such dependences of PXR intensity on energy were calculated without taking into account of MS influence on radiation characteristics.

The *Bremsstrahlung* coherent length is directly proportional to charged particle energy:

$$L_{Br} = \sqrt{\frac{4c}{\omega \overline{\theta_s^2}}},$$

where $\overline{\theta_S^2} = \frac{1}{2}\left(\frac{E_S}{E_P}\right)^2 \cdot \frac{1}{L_R}$, $E_S = 21.2$ MeV — scale energy, L_R — radiation length. Therefore, by fixing the thickness of a crystal target and changing the energy of charged particles (thus changing L_{Br}), it is possible to calculate dependences of spectral-angular density and angular distribution, and dependence of spectral maximum width on the L_0 / L_{Br} ratio (similar to shown in Fig. 1—3). Certainly, the nature of these dependences is completely different. A change of a crystal target thickness results in the change of a trajectory length where particle radiates coherently. In fact, this is its cut-off because the PXR coherent length is equal to infinity. Besides, on particle energy decrease the PXR generation is realized at increasing values of $|\alpha_B|$ (detuning parameter from exact value of Bragg angle) that in turn results in decrease of radiation intensity.

PXR spectral-angular distributions calculated for the same geometry as Fig. 1 and 2 were plotted in Fig. 4. Crystal thickness was chosen equal to 0.01 cm and polar angle of radiation was $\vartheta = 1.8$ mrad. It is evident from Fig. 4, which for 9 GeV electron beam energy distributions calculated without (curve 3) and with MS account (curve 4), practically coin-

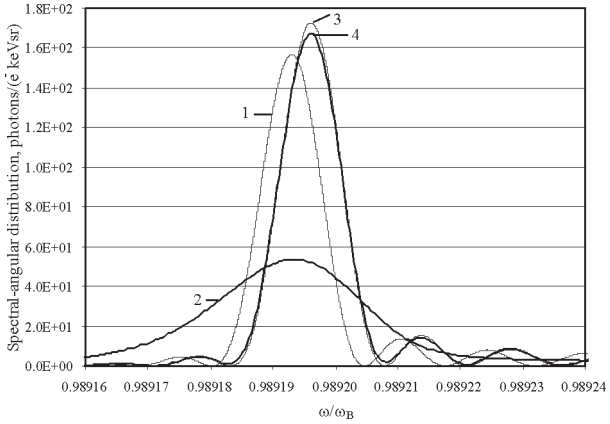

Fig. 4. PXR spectral-angular distributions plotted for various energies of electron beam: 1, 2 — 900 MeV; 3, 4 9 GeV; curves 1, 3 — calculation without MS account; 2, 4 – calculation with MS account

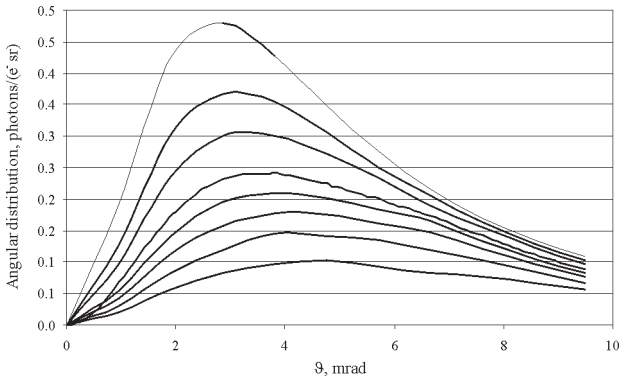

Fig. 5. PXR angular density distributions at MS presence for various beam energies. The lower curve corresponds to 300 MeV, further in upper direction: 350, 400, 450, 500, 600, 700, and 900 MeV

cides. In this case $L_{Br} = 1.22 \times 10^{-1}$ cm, i.e. $L_0 << L_{Br}$, so a situation of weak MS is realized here. Change of energy from 9 GeV down to 900 MeV yields in change of *Bremsstrahlung* coherent length to the order of magnitude, $L_{Br} = 1.22 \times 10^{-2}$ cm**.** In this case target thickness along direction of charged particle movement L_0 becomes of one order with L_{Br}. Presence of MS results in essential decrease of height and spreading of PXR peak (curve 2) in comparison with the calculations, without taking MS into account (curve 1).

The spectrum corresponding to 900 MeV appeared shifted down for $\Delta\omega \sim 5 \times 10^{-6} \omega_B$ along frequency axis relative to spectrum corresponding to 9 GeV. In the same time, shift of curve 2 relative to curve 1 as a result of MS influence for 900 MeV appeared to be just $10^{-7} \omega_B$.

Amplitudes of spectral-angular distributions without MS (curves 1 and 3) has decreased less than 1.5 times, while MS account decrease it more than four times with energy decrease from 9 GeV down to 900 MeV. Comparing spectral-angular distributions for 900 MeV energy, it is possible to see that MS account results in decrease of height of spectral-angular distribution approximately 3.2 times and its spreading ~ 2.5 times. Thus, MS presence results in decrease of PXR angular intensity.

PXR angular distributions with MS account for the geometry described above in a crystal with thickness of 0.13 cm are plotted in Fig. 5. Detector resolution was considered equal to $\Delta\varpi / \varpi_B = 10^{-3}$.

It is evident from the figure that an energy decrease to three times (from 900 down to 300 MeV) results in a decrease of maximum intensity almost five times. At the same time there is a shift of angular distribution maximum to the bigger angles from 2.9 mrad up to 4.8 mrad and spreading almost to one and half times more. Thus MS presence results in noticeable decrease of angular intensity, angular distribution spreading and to a shift of maximum in angular distribution towards the bigger angles in comparison with calculations without MS account. For example, for 300 MeV electron energy the maximum in PXR angular distribution without MS account is achieved at 2.3 mrad angle.

Study of radiation yield energy dependence is important for correct understanding of the PXR generation mechanism. This dependence, as mentioned above, has a threshold nature and its specific shape at experimental measurement in many respects is determined by the angular size of the detector. As energy decreases, the effective angle of radiation emission $\vartheta_{ph} \approx \sqrt{\gamma^{-2} - \chi_0' + \frac{\overline{\theta_s^2} L_{eff}}{2}}$ increases. Value of L_{eff} depends on crystal thickness, absorption length, Bragg angle, and radiation geometry [8].

Results of PXR quantum yield calculations for electron energy in a range from 300 up to

900 MeV are plotted in Fig. 6; angular size of detector is $9.5 \cdot 10^{-3}$ rad. The angular size of detector is $\theta_D > \vartheta_{ph}$ even for 300 MeV, that is why the detector collects practically all generated radiation and we have behaviour of quantum yield energy dependence that is "natural" for proper PXR.

Presence of MS results in a steep decrease of PXR quantum yield. For example, for 700 MeV electron energy PXR quantum yield without MS exceeds the result received with MS consideration by up to 1.5 times, for 300 MeV this value already amounts ~2.9 times.

5. CONCLUSION

Summing up, multiple scattering of charged particles in a crystal target changes considerably the characteristics of x-rays originating due to a particle passage through a single crystal. MS effect is bigger at low energies and/or thick targets and demonstrates itself in x-rays distributions spreading, monochromaticity, and quantum yield decrease. Nevertheless, PXR at low energies can provide monochromaticity of 10^{-3}—10^{-2} which is still applicable in medical imaging.

Using the approach described above, let us estimate the characteristics of PXR source, which can be produced on real medical accelerators [14]. As a rule, maximal energy of electron beam in these accelerators is equal 20—28 MeV. We have evaluated angular density of radiation for next conditions: $E_e = 25$ MeV, 33 KeV x-rays, symmetrical Laue case for (111), (220), and (400). Silicon target of L=0.01 cm was chosen which is somewhat bigger, but more real than optimal for these conditions (about $1...10 L_{Br}$, i.e. ~3...30 microns) target thickness. Angles between electron velocity direction and direction to diffraction reflex are ~6.9, 11.2, and 15.9 degrees, respectively. Angular densities for discussed cases are plotted in Fig. 7.

Integration on angular density gives us total amount of x-ray quanta on 20x20 cm area located at 1.5 m distance from the target. Appropriate amounts appeared equal to $\sim 3 \cdot 10^{-6}$, $\sim 5 \cdot 10^{-7}$, and $\sim 1 \cdot 10^{-7}$ photons/e$^-$ for (111), (220), and (400) reflexes, respectively. It is evident, that despite a decrease of radiation quantum yield at low energies, the integral amount of quanta do not decrease very drastically and the number of x-ray quanta needful for quality image can still be achieved at 0.1-0.2 A beam current.

However, to provide some margin of safety for PXR application for a medical x-ray source, it is necessary to find opportunities to increase its radiation yield. Let us consider some variants of radiation yield increase.

One of the ways to increase x-rays spectral-angular density may be the generation of radiation in a multi-wave mode, in other words, when PXR emission goes simultaneously on several systems of the crystallographic planes. In [15,16] measurements of angular distributions of PXR generated in a GaAs crystal by relativistic electrons with energies 500 and 900 MeV were reported. In these experiments the anomalies (i.e. significant intensity increase in narrow angular range), which cannot be explained by the PXR two-

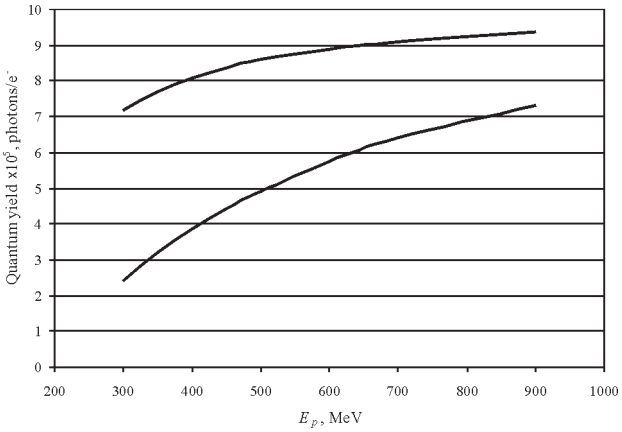

Fig. 6. PXR quantum yield dependences on electron beam energy without MS account (upper curve) and with MS account (lower curve)

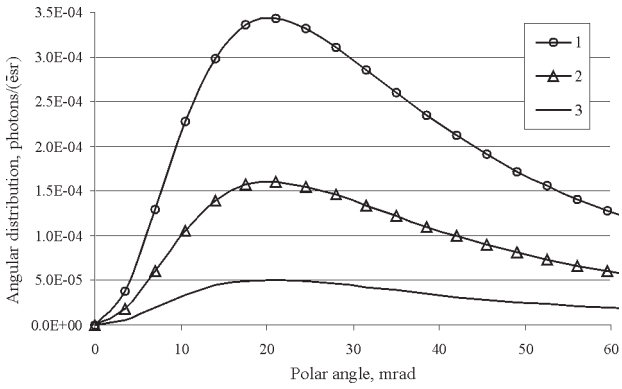

Fig. 7. Angular density for 33 keV PXR emitted by 25 MeV electrons: 1 — for (111) reflex, 2 — for (220) reflex, and 3 — for (400) reflex

wave theory [10], were observed. The analysis of geometry has shown that conditions of multi-wave diffraction were realized for emitted photons. Thorough theoretical description for experiments [15,16] was performed in [17]. In [18] demonstration of multi-wave effects in low-energy range was numerically analysed for PXR generated by 7 MeV electrons in conditions of eight-wave diffraction. Calculations have shown that, despite of strong MS of electrons at low energies, multi-wave effects may appear in PXR angular distribution and also result in the formation of a strong narrow peak in the centre of two-wave angular distribution.

Next a rather promising way for radiation spectral-angular density increase is the application of stratified (multi-layered) crystal targets [19]. PXR intensity increases up to 7—8 times in 10-layer target made of relatively thin silicon crystalline foils in comparison with monolithic target of equivalent thickness have been reported in the paper. At last, targets made of mosaic crystals should be mentioned (for example, [20]). They also can provide an increase in the intensity of x-rays.

Research of the behaviour of sophisticated targets at low energies, preferably at conditions that can provide existing medical accelerators, and determination of their optimal characteristics in this range, may lead to a practical design for a real medical monochromatic x-ray source. At the end, our results were obtained for Laue geometry, but for Bragg geometry MS influence can be somewhat weaker. Bragg geometry of PXR radiation can also provide more intensive x-ray yield. It is intended to be a subject of our further research.

ACKNOWLEDGEMENTS

Authors are very grateful to Dr. O. Missevich for fruitful discussions on x-ray imaging issues.

REFERENCES

1. *Ter-Mikaelian M.L.* High Energy Electromagnetic Processes in Condensed Media, New York: Wiley, 1972.

2. *Baryshevsky V.G., Feranchuk I.D.* Zh. Eksp. Teor. Fiz. 61 (1972) 944 (Sov. Phys. JETP 34 (1972) 502).

3. *Garybyan G.M., Yang C.* Zh. Eksp. Teor. Fiz. 61 (1972) 430 (Sov. Phys. JETP 34 (1972) 495).

4. *Adishchev Yu.N., Baryshevsky V.G., Vorobiev S.A., Danilov V.A., Pak S.D., Potylitsyn A.P., Safronov P.F., Feranchuk I.D.* Pis'ma Zh. Eksp. Teor. Fiz. 41 (1985) 295 (Sov. Phys. JETP 41 (1985) 361).

5. *Ingal V., Beliaevskaya E.* http://www.xray-site.com/knowbase/phaseradiology.html

6. The Physics of Medical Imaging / S. Webb (Ed.), Bristol: Hilger, 1978.

7. *Fiorito R.B., Rule D.W., Pierstrup M.A. et al.*, Nucl. Instrum. Meth. B 79 (1993) 758.

8. *Afanasenko V.P., Baryshevsky V.G., Lobko A.S., Panov V.V., Zuevsky R.F.* Nucl. Instrum. Meth. A334 (1993) 631.

9. *Feranchuk I.D., Ulyanenkov A., Harada J., Spence J.C.H.* Phys. Rev. E 62, #3 (2000) 4225.

10. *Feranchuk I.D., Ivashin A.V.* J. de Physique (Paris) 46 (1985) 1981.

11. *Lugovskaya O.* Characteristics of parametric x-rays in conditions of dynamical diffraction and multiple scattering, Ph. D. Thesis, NAS Institute for Physics, Minsk, Belarus, 2003.

12. *Baryshevsky V.G.* Channelling, Radiation and Reactions in Crystals at High Energies, Minsk: Belarussian University Publ., 1982 (in Russian).

13. *Baryshevsky V.G., Grubich A.O., Le Tien Hai* Sov. Phys. JETP 94 (1988) 51

14. *Abramian E.A.* Industrial Electron Accelerators, Moscow: Energoatomizdat, 1986 (in Russian).

15. *Afanasenko V.P., Baryshevsky V.G., Gradovsky O.T. et al.* Phys. Lett. 141A (1989) 311.

16. *Afanasenko V.P., Baryshevsky V.G., Gatsikha S.V. et al.* Sov. JETP. Lett. 15 (1990) 242.

17. *Stepanov S.A., Silenko A.Ya., Ulyanenkov A.P., Dubovskaya I.Ya.* Nucl. Instrum. Meth. B 117 (1996) 55.

18. *Dubovskaya I.Ya.* In: Basic and Applied Physical Studies (1986-2001) / V. Baryshevsky (Ed.), Minsk: Belarussian University Publ., 2001 (in Russian).

19. *Takashima Y., Aramitsu K., Endo I.* et al., Nucl. Instrum. Meth. B 145 (1998) 25.

20. *Fiorito R.B., Rule D.W., Maruyama X.K. et al.* Phys. Rev. Lett. 71, #5 (1993) 704.